Molecular dynamics with quantum fluctuations

Ionuţ Georgescu* and Vladimir A. Mandelshtam
Chemistry Department, University of California at Irvine, Irvine, California 92697, USA
(Received 2 July 2010; revised manuscript received 19 August 2010; published 9 September 2010)

A quantum dynamics approach, called Gaussian molecular dynamics, is introduced. As in the centroid molecular dynamics, the *N*-body quantum system is mapped to an *N*-body classical system with an effective Hamiltonian arising within the variational Gaussian wave-packet approximation. The approach is exact for the harmonic oscillator and for the high-temperature limit, accurate in the short-time limit and is computationally very efficient.

DOI: 10.1103/PhysRevB.82.094305 PACS number(s): 02.70.Ns, 31.15.xv, 52.65.Yy, 67.10.Hk

The accurate and efficient computation of dynamical properties of quantum many-body systems is a challenging task, although a number of methods exist. To name a few, the semiclassical initial value representation (SC-IVR),[1] linearized SC-IVR,[2] forward-backward IVR,[3] forward-backward semiclassical dynamics,[4] Feynman-Kleinert (FK) linearized path integral,[5] centroid molecular dynamics (CMD),[6,7] ring polymer molecular dynamics (RPMD),[8] etc.

CMD, RPMD, and the method presented here, Gaussian molecular dynamics (GMD), focus on the effect of quantum fluctuations or zero-point energy. The latter dominates in the long-time dynamics of the condensed phase while effects of quantum coherence are rapidly quenched by the interaction with the bath. The zero-point energy is therefore essential for some dynamical parameters, such as diffusion constants[9] or chemical reaction rates. Applications are not limited to nuclear dynamics at low temperatures. They also include warm, dense, nondegenerate electron plasmas, as created in atomic clusters[10] and solids[11] when exposed to intense x-ray lasers.

Conceptually akin to the CMD, the GMD maps the dynamics of an *N*-dimensional quantum system with the Hamiltonian $\hat{H}$ to that of an *N*-dimensional classical system with an effective Hamiltonian,

$$H_{\text{eff}}(x,p) = V_{\text{eff}}(x) + \frac{1}{2}p^{\mathrm{T}} m_{\text{eff}}^{-1} p, \tag{1}$$

where x and p define the pseudoclassical, respectively, coordinate and momentum vectors; m_{eff} is an effective mass tensor. The mapping is done by setting the particle density and the partition function to be the same for the two systems,

$$\rho_\beta(x) = \frac{1}{(2\pi\hbar)^N}\int dp e^{-\beta H_{\text{eff}}(x,p)} = \langle x|e^{-\beta\hat{H}}|x\rangle, \tag{2}$$

$$Z = \frac{1}{(2\pi\hbar)^N}\int dx dp e^{-\beta H_{\text{eff}}(x,p)} = \mathrm{Tr}\, e^{-\beta\hat{H}}, \tag{3}$$

which consequently defines the effective potential

$$V_{\text{eff}}(x) = -\frac{1}{\beta}\ln[\rho_\beta(x)] - \frac{1}{\beta}\ln\left\{\frac{[2\pi\beta\hbar^2]^{N/2}}{\|m_{\text{eff}}\|^{1/2}}\right\}. \tag{4}$$

The classical Hamiltonian dynamics,

$$\dot{x} = \partial H_{\text{eff}}/\partial p; \quad \dot{p} = -\partial H_{\text{eff}}/\partial x \tag{5}$$

then preserves the quantum canonical distribution. However, this classical dynamics is not necessarily related to the quantum dynamics. Moreover, the quantum-classical mapping is not unique, for example, due to the ambiguity in the choice of the mass matrix, m_{eff}. The dynamics is actually wrong, even for a one-dimensional (1D) harmonic oscillator, at finite β, if $m_{\text{eff}}=m$. Yet, we utilize this flexibility by choosing m_{eff} such that the dynamics is exact for the harmonic potential.

CMD performs the quantum-classical mapping within the path-integral Monte Carlo (PIMC) framework. In GMD we evaluate the quantum density $\rho_\beta(x)$ using the variational Gaussian wave-packet (VGW) method,[12] a recently introduced alternative to PIMC. VGW proved itself practically accurate and numerically very efficient for a wide variety of systems.[12–17] In its most consistent implementation CMD is numerically very expensive as it requires a converged PIMC calculation for each estimation of the centroid force. Subsequent developments of the CMD,[18,19] or the related RPMD,[8] though faster, may show spurious frequencies due to the presence of additional unphysical degrees of freedoms. While numerically very efficient, GMD does not introduce unphysical degrees of freedom. Furthermore, complex frequencies, as encountered in approaches based on the FK approximation,[20] do not occur in GMD.

Both CMD and GMD are exact for a harmonic oscillator and in the high-temperature limit. The CMD includes the quantum fluctuations by averaging over all ring polymers of a given centroid. The quantum fluctuations in GMD are averaged over a Gaussian wave packet.

A more recent method, the full Wigner dynamics (FWD) developed by Liu and Miller,[21] also makes use of the quantum-classical mapping. Moreover, FWD also utilizes the VGW method for calculating the Wigner transform of the Boltzmann operator $e^{-\beta\hat{H}}$. The resulting expressions to estimate the time-correlation functions are then given in terms of an average over the classical phase space. However, in its current form FWD requires one additional integral over the full configuration space, compared to the method presented here.

We illustrate here a 1D case. The multidimensional generalization of GMD is straightforward but will be presented in a forthcoming publication.

The particle density can be written in the form

$$\rho_\beta(x) = \langle x|e^{-\beta\hat{H}}|x\rangle = \langle x, \beta/2|x, \beta/2\rangle, \tag{6}$$

where

$$|x,\tau\rangle := e^{-\tau\hat{H}}|x\rangle$$

is the solution of the imaginary-time Schrödinger equation with initial condition $\langle r|x,0\rangle = \delta(r-x)$. This solution is approximated by a Gaussian wave packet,

$$\langle r|x,\tau\rangle \approx (2\pi g_\tau)^{-1/2} \exp\left[-\frac{[r-q_\tau]^2}{2g_\tau} + \gamma_\tau\right] \tag{7}$$

with variational parameters q_τ, g_τ, and γ_τ satisfying

$$q_0 = x; \quad g_0 = 0; \quad \gamma_0 = 0. \tag{8}$$

The density is then given by

$$\rho_{2\tau}(x) = \langle x,\tau|x,\tau\rangle = (4\pi g_\tau)^{-1/2} e^{2\gamma_\tau}. \tag{9}$$

Using a time-dependent variational principle, one can obtain the equations for the evolution in imaginary time,

$$\begin{aligned} dq_\tau/d\tau &= -g_\tau U'_\tau, \\ dg_\tau/d\tau &= -g_\tau^2 U''_\tau + \hbar^2/m, \\ d\gamma_\tau/d\tau &= -U_\tau - g_\tau U''_\tau/4, \end{aligned} \tag{10}$$

where U' and U'' define the first and second derivatives of the potential $U(x)$ and

$$A_\tau \equiv A_\tau(x) := \langle x;\tau|A|x;\tau\rangle \rho_{2\tau}(x)^{-1}. \tag{11}$$

The initial condition (8) are propagated from $\tau=0$ to $\tau=\beta/2$. If the potential $U(x)$ is expressed as, e.g., linear combination of Gaussians, all terms in the right-hand side of Eq. (10) can be evaluated analytically, thus making its numerical solution cheap. A detailed, full dimensional derivation of the VGW is provided in Ref. 12.

The classical limit $\hbar^2/m \to 0$ yields $q_\tau = q_0$, $g_\tau = 0$, and $\gamma_\tau = -\beta/2U(x)$, leading to the classical canonical distribution when inserted in Eq. (9). The magnitude of $\hbar^2/m$ defines the rate of broadening of the Gaussians in Eq. (10), i.e., the quantum fluctuations, which increase with decreasing temperature.

Dynamical properties are commonly expressed in terms of the time-correlation function,

$$C_{AB}(t;\beta) = \frac{1}{Z}\mathrm{Tr}[e^{-\beta\hat{H}}\hat{A}e^{i\hat{H}t/\hbar}\hat{B}e^{-i\hat{H}t/\hbar}]. \tag{12}$$

However, CMD and RPMD provide approximations for the Kubo transformed quantum time-correlation functions,[22]

$$C_{AB}^{\mathrm{Kubo}}(t;\beta) = \frac{1}{\beta Z}\int_0^\beta d\lambda \times \mathrm{Tr}[e^{(\lambda-\beta)\hat{H}}\hat{A}e^{-\lambda\hat{H}}e^{i\hat{H}t/\hbar}\hat{B}e^{-i\hat{H}t/\hbar}]. \tag{13}$$

It turns out that the most convenient choice for GMD is to deal with the symmetrized correlation function,

$$C_{AB}^{\mathrm{sym}}(t;\beta) = \frac{1}{Z}\mathrm{Tr}[e^{-\beta\hat{H}/2}\hat{A}e^{-\beta\hat{H}/2}e^{i\hat{H}t/\hbar}\hat{B}e^{-i\hat{H}t/\hbar}] \tag{14}$$

as in this case one can take advantage of the imaginary-time propagation to $\beta/2$, rather than β.

Both $C_{AB}^{\mathrm{sym}}(t;\beta)$ and $C_{AB}^{\mathrm{Kubo}}(t;\beta)$ provide the same information as the regular quantum time-correlation function $C_{AB}(t;\beta)$ and are related to each other in the Fourier space,

$$C_{AB}(\omega) = \frac{\hbar\beta\omega}{1-e^{-\hbar\beta\omega}} C_{AB}^{\mathrm{Kubo}}(\omega) = e^{\hbar\beta\omega/2} C_{AB}^{\mathrm{sym}}(\omega). \tag{15}$$

However, what makes $C_{AB}^{\mathrm{sym}}(t;\beta)$ and $C_{AB}^{\mathrm{Kubo}}(t;\beta)$ different is that they both have the same symmetries as the classical time-correlation function,

$$C_{AB}^{\mathrm{cl}}(t;\beta) = \frac{1}{Z}\int \frac{dx_0 dp_0}{2\pi\hbar} e^{-\beta H(x_0,p_0)} \times A(x_0,p_0)B(x_t,p_t), \tag{16}$$

thus making it possible to directly relate the classical and quantum dynamics in real time.

For the case when both operators are functions of position only, i.e., $\hat{A}=A(\hat{x})$ and $\hat{B}=B(\hat{x})$, for $t=0$ we can write [see Eq. (11)],

$$C_{AB}^{\mathrm{sym}}(0;\beta) = \frac{1}{Z}\int dx \rho_\beta(x) A_{\beta/2}(x) B(x). \tag{17}$$

This expression can be rewritten to reflect the structure of a classical time-correlation function at $t=0$,

$$C_{AB}^{\mathrm{sym}}(0;\beta) = \frac{1}{Z}\int \frac{dx_0 dp_0}{2\pi\hbar} e^{-\beta H_{\mathrm{eff}}(x_0,p_0)} \times A_{\beta/2}(x_0) B(x_0), \tag{18}$$

where the form of the effective Hamiltonian for the 1D case can be retrieved from Eqs. (1) and (4). We now make an *ad hoc* approximation and extend $C_{AB}^{\mathrm{sym}}(0;\beta)$ to finite times by replacing $B(x_0)$ with $B(x_t)$,

$$C_{AB}^{\mathrm{GMD}}(t;\beta) = \frac{1}{Z}\int \frac{dx_0 dp_0}{2\pi\hbar} e^{-\beta H_{\mathrm{eff}}(x_0,p_0)} \times A_{\beta/2}(x_0) B(x_t), \tag{19}$$

where (x_t,p_t) is the classical trajectory obtained by propagating the equations of motion [Eq. (5)].

Equation (5) requires an imaginary-time propagation at every point in phase space in order to obtain the quantum density and thus, the force. Each point along the real-time trajectory (x_t,p_t) is the origin of an imaginary-time trajectory q_τ with $q_0=x_t$. The real-time trajectory (x_t,p_t) is therefore connected to a second trajectory $q_{\beta/2}(t)$, which is obtained by propagating the former in imaginary time to $\beta/2$. They are interdependent since (x_t,p_t) determines $q_{\beta/2}(t)$ and vice versa.

By construction, Eq. (19) is correct in the zero-time limit $(t\to 0)$, as long as the VGW approximation of the quantum density is accurate. The next step is to adjust m_{eff} in order to make the mapping of the real-time dynamics correct at finite times as well, at least for the important limiting case of the

harmonic potential $[V(x)=\frac{1}{2}m^2\omega^2x^2]$. The VGW Eq. (10) in this case give the exact solution,

$$q_\tau = \frac{q_0}{\cosh(\hbar\omega\tau)}; \quad g_\tau = \frac{\hbar\tanh(\hbar\omega\tau)}{m\omega},$$

$$\gamma_\tau = -\frac{1}{2}\log[\cosh(\hbar\omega\tau)] - \frac{m^2\omega^2}{2\hbar^2}g_\tau q_0^2. \tag{20}$$

The effective Hamiltonian then reads

$$H_{\text{eff}}(x,p;\beta) = \frac{p^2}{2m_{\text{eff}}} + \frac{2m^2\omega^2}{\hbar^2\beta}g_{\beta/2}\frac{x^2}{2} \tag{21}$$

which is also harmonic but with a frequency that depends on m_{eff}. In order to fix its value to be equal to ω, we set

$$m_{\text{eff}} = \frac{2m^2}{\hbar^2\beta}g_{\beta/2}. \tag{22}$$

With this ansatz the time-correlation function obtained using Eq. (19) becomes exact for the harmonic oscillator at any value of β and t.

Consequently, we generalize Eq. (22) to all potentials. This local harmonic approximation makes the effective mass not only temperature but also position dependent (since for an anharmonic potential the Gaussian width $g_{\beta/2}$ depends on the position). Equation (5) then yields the explicit expressions for the real-time dynamics,

$$\dot{x} = \frac{p}{m_{\text{eff}}},$$

$$\dot{p} = \frac{1}{\beta}\frac{\partial}{\partial x}\ln[\rho_\beta(x)] + \left[\frac{p^2}{2m_{\text{eff}}} - \frac{1}{2\beta}\right]\frac{1}{m_{\text{eff}}}\frac{\partial m_{\text{eff}}}{\partial x}. \tag{23}$$

This is the main result of the present work. The quantum dynamics is mapped to the dynamics of a classical system defined by the effective Hamiltonian (1) with the effective mass [Eq. (22)]. Quantum time-correlation functions are obtained from the approximation for the symmetrized correlation function [Eq. (19)].

We illustrate the method on two 1D systems which have also been used to benchmark the CMD,[23] the RPMD,[8] FWD,[21] etc. They are the weakly anharmonic oscillator and the quartic oscillator,

$$V_1(x) = \frac{x^2}{2} + \frac{x^3}{10} + \frac{x^4}{100} \quad V_2(x) = \frac{x^4}{4}. \tag{24}$$

For both $V_1(x)$ and $V_2(x)$, we examine a low-temperature regime $\beta=8$ and a medium temperature $\beta=1$, where k_BT is comparable to the energy gap between the lowest two eigenstates.

Figure 1 shows the position autocorrelation function $C_{xx}^{\text{sym}}(t;\beta)$ for the anharmonic potential V_1. The open circles correspond to the exact result, which has been obtained by diagonalizing the Hamiltonian and estimating the symmetrized correlation functions in the basis of energy eigenstates. The GMD approximation [Eq. (19)] yields

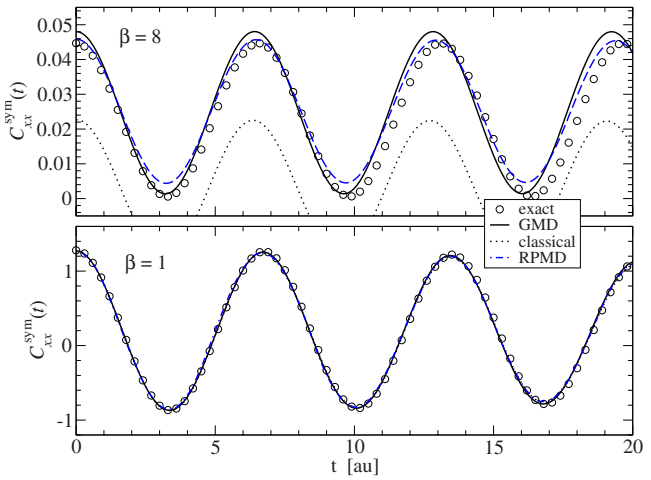

FIG. 1. (Color online) Position autocorrelation functions for $V_1(x)$, Eq. (24). Open circles: exact result; full line: GMD approach, Eq. (25); dotted line: classical result; dashed line: RPMD calculation from Ref. 8.

$$C_{xx}^{\text{GMD}}(t;\beta) = \frac{1}{Z}\int\frac{dx_0dp_0}{2\pi\hbar}e^{-\beta H_{\text{eff}}(x_0,p_0)}q_{\beta/2}x_t. \tag{25}$$

It is very close to the exact result, which is pleasing but expected because GMD is exact for the harmonic oscillator and the added anharmonicity is weak. To include the classical result for comparison, we consider the classical approximation to the Kubo-transformed time-correlation function,[22] and convert it to the symmetrized correlation function according to Eq. (15). It is totally wrong for $\beta=8$, but for $\beta=1$ it nearly coincides with the exact quantum result, again because the system is dominantly harmonic. Figure 1 also shows the RPMD results from Ref. 8, after transformation according to Eq. (15). The RPMD and GMD correlation functions behave similarly for the two temperatures considered.

Figure 2 shows the same correlation functions but for the quartic oscillator $V_2(x)$. At $\beta=8$ both GMD and RPMD,[8]

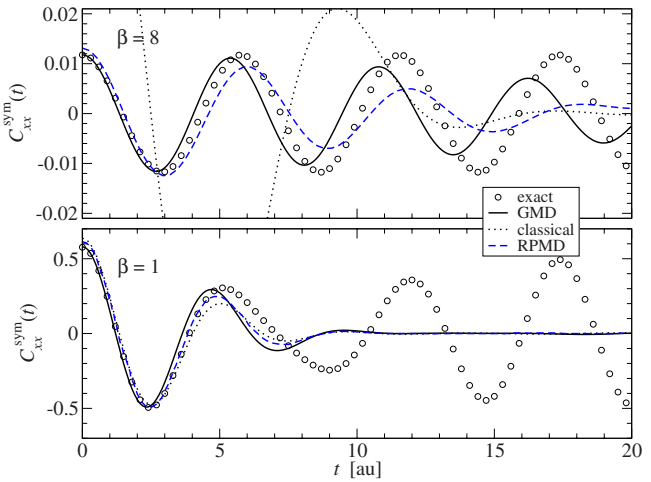

FIG. 2. (Color online) Same as Fig. 1, but for the quartic oscillator $V_2(x)$, Eq. (24).

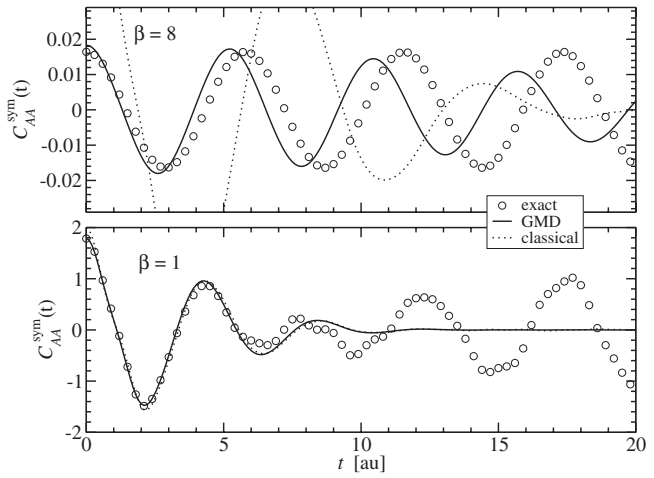

FIG. 3. Symmetrized autocorrelation function of $\hat{A}=\hat{x}^3$ for the quartic oscillator $V_2(x)$.

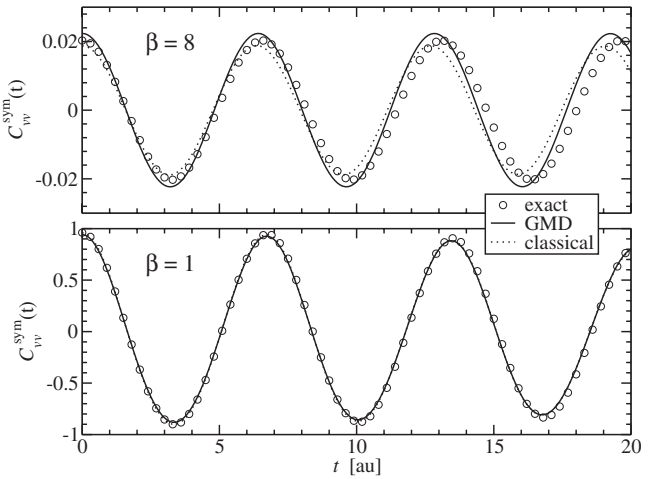

FIG. 4. Velocity autocorrelation functions for the anharmonic oscillator $V_1(x)$. Open circles: exact results; full line: GMD approach, Eq. (27); dotted line: classical results.

while reproducing quite well the oscillation period, show dephasing, a typical characteristic of a classical system. At $\beta=1$, the statistics is no longer dominated by the zero-point energy and even the classical approximation can describe well the short time dynamics, which is, again, expected.[1]

An example for a nonlinear operator, $\hat{A}=\hat{x}^3$, is provided in Fig. 3 for the same quartic oscillator $V_2(x)$.

For double well potentials, the GMD time correlation function resembles Fig. 2 as long as the average energy lies above the barrier such that tunneling is not dominant. In the opposite case, GMD faces the same problems as RPMD and CMD: relying on classical trajectories, it is impossible to penetrate the barrier and provide tunneling rates, even though the underlying "statistical" framework, the VGW or, respectively, the imaginary-time path integral, can provide the correct density in the classically forbidden region.

Because the GMD preserves the canonical distribution, correlation functions of the time derivatives of $\hat{A}$ and/or $\hat{B}$ can also be computed due to the relationship[24]

$$C_{\dot{A}\dot{B}}(t)=\frac{\partial}{\partial t}C_{\dot{A}B}(t)=-\frac{\partial}{\partial t}C_{A\dot{B}}(t)=\frac{\partial^2}{\partial t^2}C_{AB}(t), \tag{26}$$

which also holds for the quantum correlation functions. For example, the velocity-velocity correlation function can be obtained from $C_{xx}^{\mathrm{GMD}}(t;\beta)$ using this relationship. Alternatively, it can be computed directly by

$$C_{vv}^{\mathrm{GMD}}(t;\beta)=\frac{1}{Z}\int\frac{dx_0dp_0}{2\pi\hbar}e^{-\beta H_{\mathrm{eff}}(x_0,p_0)}\times\left.\frac{\partial q_{\beta/2}}{\partial q_0}\right|_{q_0=x_0}v_0v_t, \tag{27}$$

where we have used

$$\frac{\partial q_\tau}{\partial t}=\left.\frac{\partial q_\tau}{\partial q_0}\right|_{q_0=x_0}\frac{\partial x_0}{\partial t}.$$

Figures 4 and 5 depict the velocity autocorrelation function for $V_1(x)$ and $V_2(x)$, showing the same patterns of agreement with the exact calculations as the position autocorrelation function in Figs. 1 and 2.

Exact numerical solutions are not usually available for large quantum systems and assessing the accuracy of a quantum dynamical method by direct comparison with the experiment is not conclusive evidence. There is no guarantee that the employed force fields are correct and the available experimental points are quite often insufficient. Perez *et al.* have introduced a self-consistency check for quantum dynamical methods,[25] based on the fact that most of them can compute the imaginary-time correlation functions with high accuracy and that the conversion from real to imaginary time is numerically stable (unlike the opposite direction). One such imaginary-time correlation function is

$$G(\tau)=2[\langle\hat{x}^2\rangle-\langle\hat{x}\hat{x}(\tau)\rangle], \tag{28}$$

where $\hat{x}(\tau)=e^{-\tau\hat{H}}\hat{x}e^{\tau\hat{H}}$. $G(\tau)$ is related to the Fourier transform of the symmetrized velocity autocorrelation function,

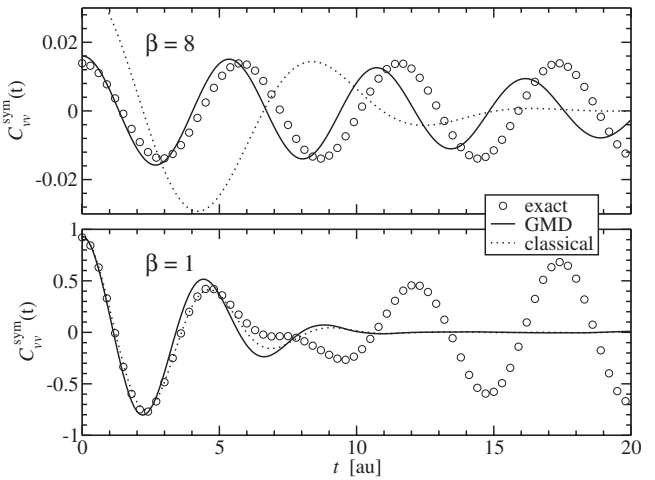

FIG. 5. Same as Fig. 4 but for the quartic oscillator $V_2(x)$.

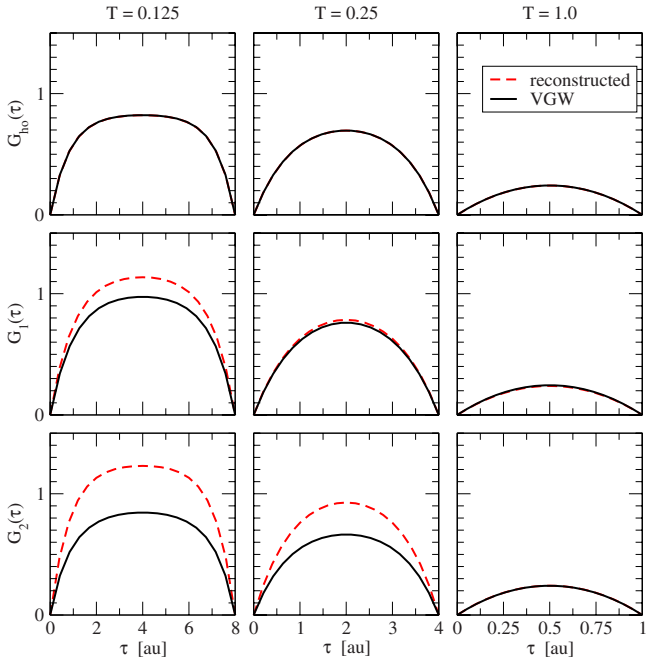

FIG. 6. (Color online) Self-consistency check. Full lines: direct evaluation of $G(\tau)$, Eq. (28); dashed lines: reconstruction from the real time domain according to Eq. (29). Upper row: a harmonic oscillator, defined in the text. Second and third row: $V_1(x)$ and, respectively, $V_2(x)$, Eq. (24).

$$G(\tau) = -\frac{1}{\pi}\int_{-\infty}^{\infty} d\omega \tilde{C}_{vv}^{\mathrm{sym}}(\omega)\{\cosh[\hbar\omega(\beta/2-\tau)] - \cosh(\hbar\omega\beta/2)\}. \quad (29)$$

Equation (29) is exponentially sensitive to high frequencies, $\omega \gtrsim 1/\hbar\beta$, and diminishes the contribution of lower ones. It neglects thereby long-time dynamics and emphasizes short-time accuracy $t \leq \hbar\beta$.

Figure 6 compares the direct evaluation of $G(\tau)$ with the VGW and the reconstruction from the real-time domain by means of Eq. (29). Test cases are the same model potentials $V_1(x)$, $V_2(x)$, and a harmonic oscillator, $V_{\mathrm{ho}}(x) = 0.7145629x^2$. At low temperatures, $\hbar\beta$ encompasses at least one oscillation period and the slightly higher oscillation frequency visible in Figs. 1 and 2 is reflected in the deviation toward larger $G(\tau)$. At high temperatures, only very short-time scales are selected, where GMD performs very well.

The GMD presented in this paper proved very powerful in estimating time-correlation functions of position-dependent operators and their time derivatives. It accounts for the zero-point energy, is accurate in the short-time limit $t \leq \hbar\beta$ and it is exact for the harmonic oscillator and in the high-temperature limit. Main applications are nondegenerate systems where the de Broglie wavelength is comparable to the range of the interaction. This includes nuclear dynamics at low temperatures or electron dynamics in warm, dense plasmas. Such systems will be investigated in more detail in future work.

While in this paper, we only tested GMD using 1D systems, for which numerically exact results are available, the method is still to be demonstrated using more challenging systems. At least for the 1D examples considered here, GMD provides the degree of accuracy comparable to that of other existing methods. The main advantage of the method will though be in its numerical efficiency. For example, compared to the FWD of Ref. 21 that utilizes the same VGW representation of the density matrix, GMD requires significantly less numerical effort (one less integral over the configuration space). When compared to the path-integral-based methods, GMD does not inflate the phase space, i.e., the corresponding classical phase space has the minimal number of degrees of freedom. This may also be viewed as an advantage, as the nonphysical degrees of freedom may in certain cases become a source of spurious dynamical effects.[26] Furthermore, the numerical efficiency of GMD over the path-integral methods relies on the efficiency in representing the quantum Boltzmann operator. For example, the ergodicity problem arising in the PIMC framework even in calculations of time-independent equilibrium properties is more severe than that in the VGW framework. Furthermore, the internal ring polymer degrees of freedom have some very high-frequency modes, thus requiring a small time step. We note Refs. 14, 15, and 27 reporting some successful applications of the VGW method to calculations of thermodynamic properties (including structural transitions) of relatively large Lennard-Jones clusters, for which the corresponding PIMC calculations are currently unfeasible.

This work was supported by the NSF under Grant No. CHE-0809108. We thank David Manolopoulos for many useful discussions, and specifically for identifying a mistake in the original version of the manuscript. We also thank Jian Liu for very useful observations, critical reading of the manuscript, and pointing out to Ref. 21.

*ionut.georgescu@uci.edu

[1] W. H. Miller, J. Phys. Chem. A **105**, 2942 (2001).
[2] H. Wang, X. Sun, and W. H. Miller, J. Chem. Phys. **108**, 9726 (1998).
[3] W. H. Miller, Faraday Discuss. **110**, 1 (1998).
[4] J. Shao and N. Makri, J. Phys. Chem. A **103**, 7753 (1999).
[5] J. A. Poulsen, G. Nyman, and P. J. Rossky, J. Chem. Phys. **119**, 12179 (2003).
[6] J. Cao and G. A. Voth, J. Chem. Phys. **99**, 10070 (1993).
[7] S. Jang and G. A. Voth, J. Chem. Phys. **111**, 2357 (1999).
[8] I. R. Craig and D. E. Manolopoulos, J. Chem. Phys. **121**, 3368 (2004).
[9] S. Habershon and D. E. Manolopoulos, J. Chem. Phys. **131**, 244518 (2009).
[10] H. Wabnitz, L. Bittner, A. R. B. de Castro, R. Döhrmann, P. Gürtler, T. Laarmann, W. Laasch, J. Schulz, A. Swiderski, K.

von Haeften, T. Möller, B. Faatz, A. Fateev, J. Feldhaus, C. Gerth, U. Hahn, E. Saldin, E. Schneidmiller, K. Sytchev, K. Tiedtke, R. Treusch, and M. Yurkov, Nature (London) **420**, 482 (2002).
[11] B. Nagler, Nat. Phys. **5**, 693 (2009).
[12] P. A. Frantsuzov and V. A. Mandelshtam, J. Chem. Phys. **121**, 9247 (2004).
[13] P. Frantsuzov, A. Neumaier, and V. A. Mandelshtam, Chem. Phys. Lett. **381**, 117 (2003).
[14] C. Predescu, P. A. Frantsuzov, and V. A. Mandelshtam, J. Chem. Phys. **122**, 154305 (2005).
[15] P. A. Frantsuzov, D. Meluzzi, and V. A. Mandelshtam, Phys. Rev. Lett. **96**, 113401 (2006).
[16] J. Deckman, P. A. Frantsuzov, and V. A. Mandelshtam, Phys. Rev. E **77**, 052102 (2008).
[17] P. A. Frantsuzov and V. A. Mandelshtam, J. Chem. Phys. **128**, 094304 (2008).
[18] J. Cao and G. A. Voth, J. Chem. Phys. **101**, 6168 (1994).
[19] T. D. Hone, P. J. Rossky, and G. A. Voth, J. Chem. Phys. **124**, 154103 (2006).
[20] R. P. Feynman and H. Kleinert, Phys. Rev. A **34**, 5080 (1986).
[21] J. Liu and W. H. Miller, J. Chem. Phys. **126**, 234110 (2007).
[22] R. Kubo, J. Phys. Soc. Jpn. **12**, 570 (1957).
[23] S. Jang and G. A. Voth, J. Chem. Phys. **111**, 2371 (1999).
[24] R. Zwanzig, *Nonequilibrium Statistical Mechanics*, 1st ed. (Oxford University Press, New York, 2001).
[25] A. Perez, M. E. Tuckerman, and M. H. Muser, J. Chem. Phys. **130**, 184105 (2009).
[26] S. Habershon, G. S. Fanourgakis, and D. E. Manolopoulos, J. Chem. Phys. **129**, 074501 (2008).
[27] J. Deckman and V. A. Mandelshtam, Phys. Rev. E **79**, 022101 (2009).